A 1- and 2-D ^{19}F MAS NMR Study of Fluoride-Ion Mobility in α PbF_2

Francis Wang and Clare P. Grey*

Contribution from the Department of Chemistry, State University of New York at Stony Brook, Stony Brook, New York 11794-3400

Received July 11, 1997. Revised Manuscript Received October 24, 1997

Abstract: One- and two-dimensional ^{19}F high-speed MAS NMR are used to probe motion of the fluorine sublattices in the fluoride-ion conductors α PbF_2 and potassium fluoride-doped α PbF_2. The two crystallographic sites F(1) and F(2) are resolved in the ^{19}F spectrum of the pure material and are assigned on the basis of their $^{207}Pb-^{19}F$ J-coupling. A resonance from fluoride-ions jumping rapidly between the two sites is also observed above 120 °C, which increases in intensity as the temperature is raised. The resonance from the mobile fluoride-ions is observed at room temperature for the α PbF_2 sample containing potassium impurities and for samples that have been intentionally doped with KF by direct reaction of KF and PbF_2. The correlation times of the rigid and mobile fluoride-ions in these samples differ by more than 2 orders of magnitude, and 2-D magnetization exchange methods show that the exchange between these two sets of fluoride-ions is negligible. The vacancies produced by potassium doping appear to remain closely associated with the potassium defects at low temperatures, and the mobile fluoride-ions at these temperatures are assigned to fluoride-ions near the potassium defects. In contrast, in the pure, or more uniformly potassium-doped, materials, the vacancies are more uniformly distributed over the solid, resulting in spectra with a narrower range of correlation times for fluoride-ion motion. Finally, a low activation energy conduction pathway between F(1) and F(2) sites along the *y*-axis is proposed to rationalize the rapid F(1)↔F(2) fluoride-ion diffusion.

Introduction

The defects formed in doped crystalline ionic-conducting solids have been the subject of considerable study, in part due to the enhanced ionic transport properties of many of these materials.[1−5] Descriptions of the local defect structure in these materials have largely been proposed as a result of macroscopic measurements of diffusion and conductivity, NMR spin−lattice relaxation times, and diffraction data.[6−8] Magic angle spinning (MAS) NMR provides an ideal method to probe the local order and motion of the defective sublattices of ionic conductors directly.[9−13] Many of these studies have involved the study of cation mobility of monovalent cations such as lithium and sodium in, for example, crystalline and amorphous silicates, aluminum fluorides, layered materials, and ceramics.[11−14] The relatively recent development of high speed MAS probes, capable of spinning over 20 kHz, has allowed strongly dipolar coupled systems such as inorganic fluorides to be probed, and a limited number of one-dimensional (1-D) high-resolution spectra of inorganic fluorides have been reported.[15]

We recently published a preliminary communication demonstrating the use of ^{19}F MAS NMR to study the fluoride-ion mobility of α PbF_2.[9] α PbF_2 has been considerably less well studied than the solid-electrolyte β PbF_2. α PbF_2 is a moderate anion-conductor with conductivities between 3.9 and 5.3×10^{-6} Ω^{-1} cm^{-1} at 100 °C[6] and adopts the $PbCl_2$ structure.[16] Fluoride-ion diffusion is thought to occur via a vacancy mechanism.[17] Doping with monovalent cations such as potassium results in an increased ionic-conductivity of, in some cases, several orders of magnitude.[6] In this paper, we report a detailed one- and two-dimensional ^{19}F MAS NMR study of the effect of potassium

* To whom correspondence should be addressed.

(1) Adler, S. B.; Russek, S.; Reimer, J.; Fendorf, M.; Stacy, A.; Huang, Q.; Santoro, A.; Lynn, J.; Baltisberger, J.; Werner, U. *Solid State Ionics* **1994**, *68*, 193-211.

(2) Adler, S. B.; Smith, J. W. *J. Chem. Soc., Faraday Trans.* **1993**, *89*, 3123−3128.

(3) Shareefuddin, Md.; Jamal, Md.; Chary M. N. *Solid State Ionics* **1996**, *83*, 229−233.

(4) Eicken, J.; Gunsser, W.; Karus, M.; Meyer, A.; Murin, I. V. *Solid State Ionics* **1994**, *72*, 7−11.

(5) Chang, H.; Engelsberg, M.; Lowe, I. J. *Solid State Ionics* **1981**, *5*, 609−612.

(6) Liang, C. C.; Joshi, A. V. *J. Electrochem. Soc.* **1975**, *122*, 466−470.

(7) Schulz, H. In *Solid State Chemistry 1982 − Proceedings of the Second European Conference*; Metselaar, R., Heijligers, H. J. M., Schoonman, J., Eds.; Elsevier Scientific Publishing Company: Amsterdam, 1983.

(8) Roos, A.; Aalders, A. F.; Schoonman, J.; Arts, A. F. M.; Wijn, H. W. *Solid State Ionics* **1983**, *9−10*, 571−574.

(9) Wang, F.; Grey, C. P. *J. Am. Chem. Soc.* **1995**, *117*, 6637−6638.

(10) Wang, F.; Grey, C. P. *Chem. Mater.* **1997**, *9*, 1068−1070.

(11) Xu, Z.; Stebbins, J. F. *Science* **1995**, *270*, 1332−1334.

(12) Stebbins, J. F.; Xu, Z.; Vollath, D. *Solid State Ionics* **1995**, *78*, L1-L8.

(13) Spearing, D. R.; Stebbins, J. F.; Farnan, I. *Phys. Chem. Minerals* **1994**, *21*, 373−386.

(14) Smaihi, M.; Petit, D.; Gourbilleau, F.; Chaput, F.; Boilot, J. P. *Solid State Ionics* **1991**, *48*, 213. Mustarelli, P.; Scotti, Sergio; V., Marco; G., Prashant R. *Solid State Ionics* **1990**, *39*, 217−24. Eckert, H.; Zhang, Z.; Kennedy, J. H. *Mater. Res. Soc. Symp. Proc.* **1989**, *135*, 259. Nairn, K. M.; Forsyth, M.; Greville, M.; MacFarlane, D. R.; Smith, M. E. *Solid State Ionics* **1996**, *86*, 1397. Wong, S.; Vasudevan, S.; Vaia, R. A.; Giannelis, E. P.; Zax, David B. *J. Am. Chem. Soc.* **1995**, *117*, 7568.

(15) For example, Moran, L. B.; Berkowitz, J. K.; Yesinowski, J. P. *Solid State Nucl. Magn. Reson.* **1993**, *1*(6), 307. Moran, L. B.; Berkowitz, J. K.; Yesinowski, J. P. *Phys. Rev. B* **1992**, *45*(10), 5347. Clark, J. H.; Goodman, E. M.; Smith, D. K.; Brown, S. J.; Miller, J. M. *J. Chem. Soc., Chem. Commun.* **1986**, 657−658. Kreinbrink A. T.; Sazavsky C. D.; Pyz, J. W.; Nelson D. G. A.; Honkonen R. S. *J. Magn. Reson.* **1990**, *88*, 267−276.

(16) Boldrini, P.; Loopstra, B. O. *Acta Crystallogr.* **1967**, *22*, 744−745.

(17) Mahajan, M.; Rao, B. D. N. *Chem. Phys. Lett.* **1971**, *10*, 29−30.

S0002-7863(97)02312-3 CCC: $15.00
Published on Web 01/22/1998

Figure 1. Schematic representation of the 2-D magnetization exchange pulse sequence. The pulse sequence employs three 90° pulses, separated by the evolution time (t_1) and the mixing time (t_m). The spectrum is acquired (t_2) following the third pulse.

doping on the fluoride-ion mobility. We show that ^{19}F MAS NMR is extremely sensitive to the distributions of the dopant potassium ions within the lattice and that very different fluoride-ion motion is obtained depending on preparation conditions.

Chemical exchange processes occurring between sites with differing chemical shifts result in characteristic NMR line shapes, when the rate of the exchange process enters the so-called intermediate regime of motion.[18] Thus in principle, if the individual fluorine crystallographic sites can be resolved in an ^{19}F MAS NMR spectrum of a fluoride, one-dimensional methods can be used to obtain correlation times between the different fluoride-ion sublattices, when the frequency of the motion is of the same order of magnitude as the separation in frequency between the different resonances of the sublattices. This was demonstrated in our earlier papers on α PbF_2 and LaF_3.[9,10] For the case of a simple two-site exchange process between two different sites of equal populations, a broadening of the two resonances is initially observed, given by $(\tau_c\pi)^{-1}$, where τ_c is the correlation time, as the rate of exchange approaches the difference in frequency between the two sites and enters the intermediate regime of motion.[18] As the rate of exchange increases, the two resonances coalesce, and the correlation time at coalescence is a function of the chemical shift difference between the two resonances ($\nu_A - \nu_B$):

$$\tau_{coal.} = 2^{1/2}/\pi(\nu_A - \nu_B) \quad (1)$$

As the correlation time decreases, the line width of the resonance decreases, and when the exchange rate is close to the fast-regime, a single Lorentzian line is observed with a line width given by

$$\Delta\nu_{1/2} = 1/2\pi(\nu_A - \nu_B)^2\tau_c \quad (2)$$

where k_r is the first-order rate constant for exchange ($= 1/\tau_c$). In the fast regime of motion ($k_r \gg (\nu_A - \nu_B)$), the line width is no longer sensitive to changes in the exchange rate. The line shapes that are observed for two-site exchange can be readily simulated, allowing correlation times for specific jump processes to be extracted.

Another NMR technique that can be used to probe chemically exchanging systems is 2-D magnetization exchange NMR spectroscopy.[19] 2-D magnetization exchange spectroscopy is widely used in solution NMR spectroscopy to probe correlation times in the slow regime of motion ($k_r \ll (\nu_A - \nu_B)$), where again the 1-D spectrum is no longer sensitive to the exchange rate. The standard 2-D magnetization exchange pulse sequence is shown in Figure 1. The first $\pi/2$ pulse excites the ^{19}F spins, which then evolve during the evolution period t_1. The second $\pi/2$ pulse returns the magnetization along the direction of the static magnetic field. Exchange takes place predominantly during the subsequent mixing period, t_m, before the third pulse returns the magnetization to the transverse plane for detection. Equations can be written for two site exchange (A ↔ B) with rate, k, in terms of M_z^A and M_z^B, the magnetization of spins A and B at the end of the mixing period[19]

$$M_z^A(t_1,t_m) = -1/2M_o^A[(1 + e^{-2kt_m})\cos\nu_A t_1 + (1 - e^{-2kt_m})\cos\nu_B t_1]e^{-T_1 t_m} \quad (3)$$

where T_1 is the spin−lattice relaxation time. An analogous expression can be written for M_z^B. The final $\pi/2$ pulse returns the magnetization into the xy plane for detection, and two resonances with frequencies ν_A and ν_B are detected, whose amplitudes are directly proportional to M_z^A and M_z^B. Magnetization which has precessed at ν_A in t_1 and resumes precession at ν_B after t_m will appear as a cross-peak at $\omega_1 = \Omega_A$ and $\omega_2 = \Omega_B$. Diagonal peaks result from magnetization that has not migrated from one site to another. The amplitudes of the peaks in the 2D spectrum can readily be calculated[19] and are given by

$$a_{AA}(t_m) = a_{BB}(t_m) = 1/2[1 + e^{-2kt_m}]e^{-T_1 t_m} \quad (4)$$

$$a_{AB}(t_m) = a_{BA}(t_m) = 1/2[1 - e^{-2kt_m}]e^{-T_1 t_m} \quad (5)$$

where a_{AA} and a_{BB}, and a_{AB} and a_{BA} are the amplitudes of the diagonal peaks and cross-peaks, respectively. Combining and rearranging these equations allows the rate, k, to be obtained from the cross-peak and diagonal amplitudes:[19]

$$(a_{AA} - a_{AB})/(a_{AA} + a_{AB}) = e^{-2kt_m} \quad (6)$$

A 2-D magnetization exchange experiment has recently been applied to study lithium-ion motion in a crystalline lithium silicate ionic-conductor and rates for exchange between different cation sites were extracted.[11] In this paper, we report the use of the technique to study fluoride-ion motion in α PbF_2 and to demonstrate that domains of mobile fluoride-ions exist in some of the doped materials, which do not undergo significant exchange with the rest of the rigid lattice.

Experimental Section

Materials Preparation. Two commercially available samples of α PbF_2 (Aldrich, nominal purity 99+% and Alfa, nominal purity 99.9%) were used. Impurity levels, as provided from the two chemical companies, were based on different chemical analysis. The figure determined from Aldrich was determined from the metals content, while that from Alfa was based on the fluoride-ion content. ^{19}F NMR and further chemical analyses (see below) indicated that the Aldrich material contained lower levels of cation impurities, and hence, this purer sample was used in all the syntheses reported below. X-ray powder diffraction of both samples gave powder diffraction patterns consistent with the α PbF_2 structure, and no impurity phases were detected. Anion deficient potassium-doped α PbF_2 samples were prepared by two different methods. In the "dry" method, appropriate amounts of α PbF_2 and KF were mixed together and fired under vacuum at 250 °C for 5 h. In an attempt to distribute the small concentration of potassium cations more evenly throughout the crystallites, a wet or solution method was also used. The KF was first dissolved in a minimum of distilled water. The KF solutions were then added to appropriate amounts of α PbF_2, to coat the particles. The wet slurry was then slowly heated under vacuum to 250 °C, to remove the water, and was held at 250 °C for a further 8 h. ^{19}F NMR of the KF-doped samples indicated complete reaction and a resonance from KF could not be detected. No new phases were detected in the X-ray powder diffraction patterns. All samples were stored in a drybox, under inert nitrogen atmosphere, to

(18) Abragam, A. *The Principles of Nuclear Magnetism*; Oxford University Press: Oxford, UK, 1961.

(19) Jeener, J.; Meier, B. H.; Bachmann, P.; Ernst, R. R. *J. Chem. Phys.* **1979**, *71*, 4546−4553.

Table 1. α PbF_2 Sample Notation Used in This Paper, α PbF_2 Source, KF Dopant Levels (mol %), and Method of KF Incorporation

sample	source	%age KF	method of incpn
PbF_2−1	Aldrich		
PbF_2−2	Alfa		
PbF_2−w	Aldrich	0.2	wet
PbF_2−d	Aldrich	0.2	dry

Table 2. Composition of the Two Samples of α PbF_2-1 (Aldrich 99+%) and α PbF_2-2 (Alfa 99.9%)[a]

sample	sputter time (min)	F	O	C	Pb	K
α PbF_2−1	0	41.0	11.1	21.8	26.1	
α PbF_2−1	7	62.0	0.0		38.0	
α PbF_2−1	15	61.7	0.0		38.3	
α PbF_2−2	0	41.0	8.5	17.9	22.9	9.7
α PbF_2−2	7	63.9	0.0		35.6	<0.5
α PbF_2−2	15	64.1	0.0		34.0	<0.2

[a] As Determined from X-ray Photoelectron Spectroscopy, as a Function of the Sputtering Time. Elemental Analyses Are Given as Atomic Weight Percentages.

minimize effects of moisture and oxygen. The details of the preparations, doping levels, and labeling of the samples used in this paper are shown in Table 1.

Elemental Analysis: X-ray Photoelectron Spectroscopy. This was used to characterize the surface composition of the lead fluoride samples. Data were acquired with a Physical Electronics Model 5701 LSci spectrometer with a monochromatic aluminum X-ray source. An analysis region of 2 × 0.8 and 0.8 × 0.8 mm^2 before, and after sputtering, respectively, an exit angle of 45°, and an electron acceptance angle of ±7° were used.

Electron Microprobe Analysis. A CAMECA Camebax Micro (WDS) scanning electron X-ray microprobe analyzer, equipped with an EDS spectrometer for semiquantitative sample analysis for elements with $Z > 8$, was used. Analysis was performed with an approximately 1 micron electron beam.

NMR Measurements. ^{19}F NMR measurements were performed on a 360 MHz Chemagnetics spectrometer at an operating frequency for ^{19}F of 338.75 MHz. Use of a double resonance Chemagnetics pencil probe equipped with 3.2 mm rotors, allowed spinning speeds of up to 24 kHz to be attained. The room-temperature spectra of α PbF_2-1, collected at 29 kHz, were acquired with a Chemagnetics prototype probe with 2.5 mm rotors. ^{19}F MAS NMR spectra were referenced to CCl_3F at 0 ppm. The 2-D magnetization exchange pulse sequence, that was used in all 2-D experiments, is shown in Figure 1. Spectra are recorded for regular increments of t_1; TPPI was used to acquire phase sensitive spectra in the t_1 dimension.

NMR Simulations. Chemical exchange simulations were performed with MATHEMATICA@, using an expression for the line shape of a set of two spins with equal populations undergoing chemical exchange.[20]

Results

Elemental Analysis. X-ray photoelectron spectroscopy (Table 2) was performed on both the samples of α PbF_2 to investigate the levels of impurities present on, or near, the surface of the crystallites. Although both surfaces contained a significant amount of oxygen, none was detected in either sample after they had been subjected to extended ion sputtering. The α PbF_2-2 contained a relatively high concentration of potassium at the surface, while none was detected in α PbF_2-1. Trace amounts of potassium (<0.2 at. %) were still detected in α PbF_2-2 even after 15 min of sputtering.

Electron microprobe analysis was performed in point mode over a series of crystallites of approximately 2 μm in length.

(20) Harris R. K. *Nuclear Magnetic Resonance Spectroscopy: A Physicochemical View*; Longman Scientific & Technical: Essex, UK, 1983.

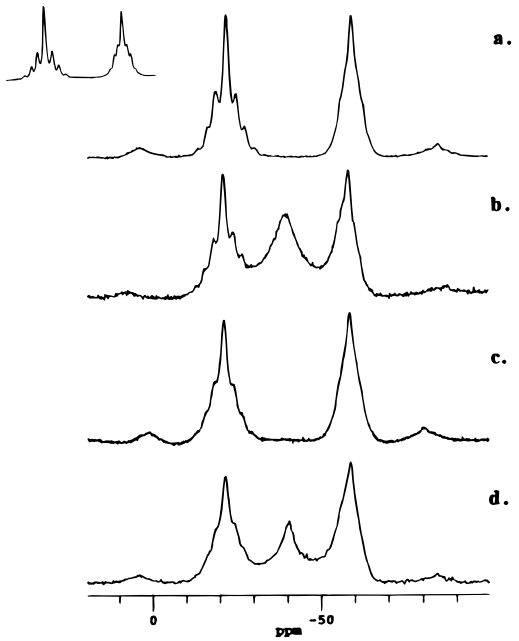

Figure 2. Room temperature very fast ^{19}F MAS NMR spectra of a. α PbF_2-1 at 20 kHz (insert at 29 kHz), b. α PbF_2-2 at 23 kHz, c. α PbF_2-w at 20 kHz, and d. α PbF_2-d at 20 kHz.

Only elements with $Z \geq 9$ can be detected with the setup used, due to absorption of the emission from light elements by the detector window, and accurate quantitative analysis of trace amounts of elements with $Z > 9$ is difficult. Nonetheless, the analysis showed that the α PbF_2-1 sample was relatively free of impurities, while α PbF_2-2 contained trace amounts of potassium. Variation in the potassium concentration was observed for the different crystallites: negligible potassium concentrations were observed for some regions, while others contained significant amounts. Different morphology was also seen for the two samples. α PbF_2-1 consists of regular needle-shaped polycrystallites, while the α PbF_2-2 particles show more variations in morphology and are comprised of mainly smaller rounder particles which appear to consist of smaller agglomerated particles. The differences in morphology suggest two different methods of manufacture.

One-Dimensional ^{19}F MAS NMR. Figure 2a,b shows the 1-D room temperature ^{19}F MAS NMR spectrum of α PbF_2-1 and α PbF_2-2, collected at spinning speeds of 20 kHz; the ^{19}F spectrum of α PbF_2-1, collected at 29 kHz, is shown in the insert. The spectrum collected at 29 kHz shows an increased resolution for the two resonances at −20.5 and −57.7 ppm, which were previously assigned to the crystallographic sites F(1) and F(2), respectively, on the basis of their different ^{207}Pb-^{19}F *J*-coupling patterns.[9] Seven major peaks (separated by 1.0 kHz) are observed for the multiplet at −20.5 ppm. Deconvolution of the septet yielded intensity ratios of 2.0:7.4:16.6:49.9:16.7:7.6:2.0, which can be compared to the previously reported septet ratio intensity of 1.5:7:17:49:17:7:0.2 obtained for α PbF_2-2.[9] F(1) is coordinated to four lead atoms, and thus, five magnetically inequivalent environments are possible for F(1): $F(^{207}Pb)_x(Pb)_{4-x}$, (where Pb represents lead nuclei with no nuclear spin; $x = 0-4$), which give rise to a singlet, doublet, triplet, quartet and quintet for $x = 0$, 1, 2, 3, and 4, respectively. The ^{207}Pb-^{19}F *J*-coupling for F(1) is given by twice the separation of the peaks in the multiplet and is therefore 2.0 kHz. Given a natural abundance for ^{207}Pb of 22.6%, probabilities for the occurrence of each of these environments of 35.8, 41.9, 18.4, 3.6, and 0.3, respectively, can be calculated. Thus, a nonet with

intensities 0.02:0.45:4.7:21.9:45.1:21.9:4.7:0.45:0.02 is predicted. Both samples show reasonable agreement between the calculated and experimentally observed values, although the central peak is slightly more intense than predicted. The outer satellites of this multiplet have very small intensities and were not detected experimentally. Nine peaks are observed for the F(2) site at −57.7 ppm with intensities, obtained by deconvolution, of 0.3:1.1:9.6:14:42:14:101.0:0.3. In contrast to the F(1) site, the resonances of the nonet at −57.7 ppm are not evenly spaced, significant differences in the splittings between the first and second sets of satellite peaks of 0.75 and 0.50 kHz, being observed, respectively. The F(2) site in the α PbF_2 structure is coordinated to five lead atoms and has Pb−F bond lengths that vary from 2.41 to 3.03 Å. The variations in Pb−F bond lengths should lead to a more complex J-coupling pattern in comparison to that from F(1) which has much smaller variations in Pb−F bond lengths (±0.1 Å). The lower intensity of the center frequency is also consistent with a higher coordination number for fluorine.

The spectrum of α PbF_2-2 shows an additional resonance at −39.0 ppm which is intermediate in chemical shift between the resonances from the F(1) and F(2) sites. We previously assigned this resonance to a subset of fluoride-ions that are undergoing rapid jumps between the F(1) and F(2) fluorine sites, at rates that are larger than the frequency separation of the two resonances (i.e., 12.6 kHz).[9] The fluoride-ion motion results in a reduced ^{19}F homonuclear dipolar coupling constant, and no spinning sidebands are observed for this resonance, in contrast to the resonances at −20.5 and −57.7 ppm. The number of mobile fluoride-ions can be obtained by integrating the spectrum and is equal to 32 ± 2% of the total number of fluoride-ions.

The room temperature ^{19}F MAS NMR spectra of PbF_2-w and PbF_2-d collected at 20 kHz are shown in Figure 2c,d, respectively. The KF dopant levels (0.2 mol %) were chosen so that they are similar to the impurity levels detected close to the surface of α PbF_2-2. Only two resonances are observed at −20.5 and −57.7 ppm from the F(1) and F(2) crystallographic fluorine sites in the spectrum of PbF_2-w, and the resonance from the mobile fluoride-ions is not observed. The ^{207}Pb-^{19}F *J*-coupling, however, is no longer so clearly resolved for the F(1) site. This observation may be attributed to some increased fluoride-ion motion, over that detected in α PbF_2-1.

F(1)↔F(1) and/or F(2)↔F(2) jump processes will lead to a change in the numbers and spin states of the ^{207}Pb nuclei that are coupled to the ^{19}F nuclei and an averaging of the *J*-coupling pattern will result if the frequency of the motion is of the same order or larger than the *J*-coupling. As the rate for the F(1)↔F(1) fluoride-ion motion approaches the ^{207}Pb-^{19}F *J*-coupling frequency (i.e., 2 kHz), a broadening of the peaks within the *J*-multiplet will be observed. F(1)↔F(2) exchange, however, will also give rise to broadening of the F(1) multiplets but in contrast to F(1)↔F(1) exchange will also lead to an increase in the line width of the ^{207}Pb decoupled resonance. Comparison of the F(1) and F(2) line widths of the ^{207}Pb decoupled spectra of α-PbF_2-w and α-PbF_2-1 show only a slight broadening of 55 Hz in the α-PbF_2-w F(1) and F(2) line widths. The slight increase in line width is consistent with an increased F(1)↔F(2) exchange process, but small contributions from F(1)↔F(1) and F(2)↔F(2) jump processes cannot be totally excluded.

The room temperature ^{19}F MAS NMR spectrum of α PbF_2-d (Figure 2d) shows two broad resonances at −20.5 and −57.7 ppm and a narrower resonance at −39.0 ppm. The ^{207}Pb-^{19}F *J*-coupling can be discerned, but like α PbF_2-w, the ^{207}Pb-^{19}F *J*-coupling is not as well resolved as in the α-PbF_2-1 spectrum. A slight increase (86 Hz) in the line width of the F(1) and F(2) sites is seen, in comparison to the spectrum of α PbF_2-1, in the ^{207}Pb decoupled spectrum. As was the case for α PbF_2-w, this is likely a result of small increases in F(1)↔F(2) exchange rates, although a small contribution from F(1)↔F(1)/F(2)↔F(2) jump processes cannot be completely ruled out. Again, the presence of spinning sidebands and some fine structure in the F(1) and F(2) resonances suggest that the increases in fluoride-ion motion are small. Like α PbF_2-2, the spectrum of α PbF_2-d shows an additional resonance at −39.0 ppm, with no associated spinning sidebands, that accounts for 13 ± 2% of the total number of fluoride-ions. This is due to a subset of fluoride-ions that are undergoing rapid jumps between the F(1) and F(2) fluorine sites.

Figure 3 shows the variable temperature ^{19}F and ^{207}Pb decoupled ^{19}F MAS NMR spectra of α PbF_2-1. The ^{19}F spectra remain unchanged at temperatures below 120 °C. The ^{207}Pb-^{19}F *J*-coupling is still clearly resolved at this temperature, indicating that the fluoride-ions that give rise to the F(1) and F(2) resonances remain rigid. At 120 °C, a small resonance at −39.0 ppm is detected, which increases in intensity as the temperature increases. By 200 °C, this resonance accounts for 26 ± 2% of the total number of fluorine and overlaps with the resonances at −20.5 and −57.7 ppm. The ^{207}Pb decoupled spectra shows a small increase in line width (51 Hz) of the F(1) and F(2) sites at 160 °C. The F(1) and F(2) line widths continue to increase as the temperature is raised: the F(1)↔F(2) exchange rate of the rigid fluoride-ions is gradually approaching 12.6 kHz and entering the intermediate regime of motion.

The line shapes are not consistent with a simple two-site exchange process but result from multiple regimes of motion. For example, at 250 °C, a complex line shape is observed: the central resonance is due to fluoride-ions undergoing F(1)↔F(2) jumps in the intermediate regime of motion, but with a frequency greater than that required for coalescence, i.e., of more than $\pi(\nu_{F(1)} - \nu_{F(2)})/2^{1/2}$ (28 kHz) (see eq 2). No spinning sidebands are observed for this resonance, consistent with rapid fluoride-ion motion. No *J*-coupling is discerned for the F(1) and F(2) resonances, indicating that the fluoride-ions giving rise to these resonances are undergoing motion with a rate of more than $J x \pi/2^{1/2}$ (approximately 4 kHz). Line shape simulations (see below) allow more detailed analyses of the correlation times and allow estimations of the populations of the ions undergoing the different regimes of motion.

The variable temperature ^{19}F MAS NMR spectra of α PbF_2-2 (Figure 4) shows a gradual increase in intensity and a decrease in the line width of the resonance at −39.0 ppm, as the temperature is increased. By 230 °C, only this resonance is observed. Although the intensity of the F(1) and F(2) resonances gradually decreases, the ^{207}Pb-^{19}F *J*-coupling remains well resolved throughout. The spectra are consistent with a gradual increase in the fraction of fluoride-ions that are undergoing fluoride-ion motion close to the fast regime of motion. A reduction of the temperature, below room temperature, results in a gradual decrease in the intensity of the resonance at −39.0 ppm, and at 6 °C, the resonance can no longer be detected. The motion of all the fluoride-ions is therefore in the slow exchange limit by 6 °C.

The spectra of the potassium-doped α PbF_2 samples produced by "wet" and "dry" methods show very different behavior as a function of temperature. An additional broad component, between the F(1) and F(2) resonances, is observed in the ^{19}F MAS NMR spectra of α PbF_2-w (Figure 5) as the temperature increases, due to fluoride-ion exchange in the intermediate

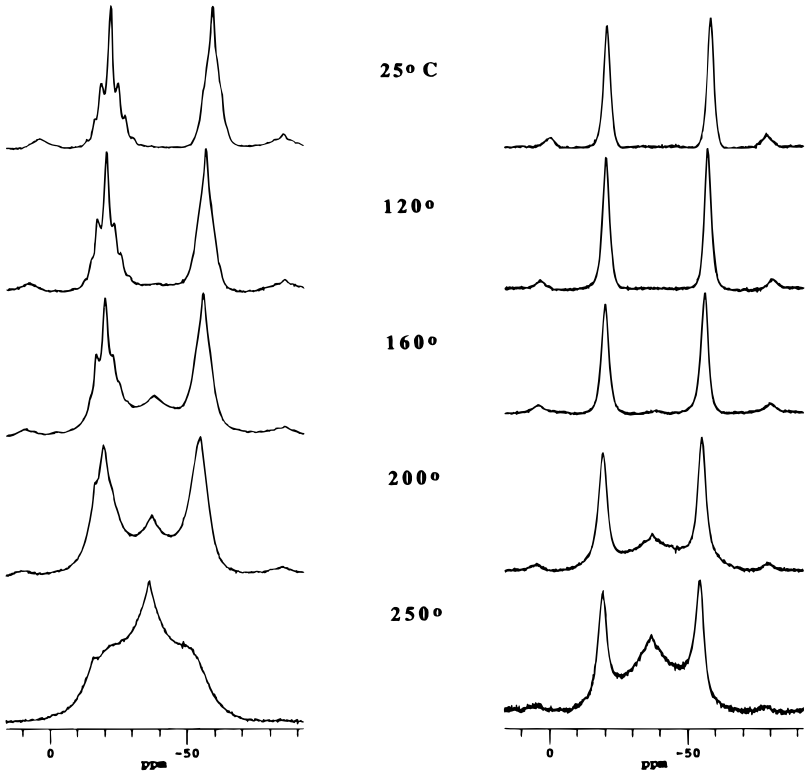

Figure 3. Variable temperature ^{19}F (left column) and ^{207}Pb decoupled (right column) ^{19}F MAS NMR spectra of α PbF_2-1 collected at room temperature, 120, 160, 200, and 250 °C at spinning speeds 20−21 kHz.

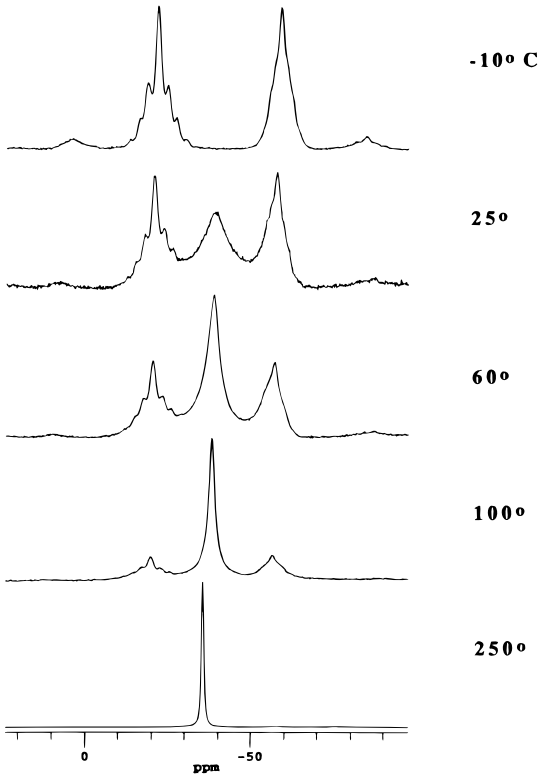

Figure 4. Variable temperature ^{19}F MAS NMR spectra of α PbF_2-2 collected at −10, 25, 60, 100, and 250 °C at spinning speeds 20−21 kHz.

regime of motion. By 80 °C, the broad resonance at −39.0 ppm accounts for 80 ± 2% of the total amount of fluorine. As the temperature increases, the resonance at −39.0 ppm narrows and increases in intensity, while the resonances at −20.5 and −57.7 ppm decrease in intensity and increase in line width slightly. Analysis of the populations and correlation times of the different regimes of motion are provided by line shape simulations (see below). At temperatures above 140 °C, only a single resonance at −39.0 ppm is observed. The fluorine motion observed at high temperatures can be "frozen out" by lowering the temperature. The decrease in fluoride-ion motion at temperatures below −10 °C is evident in the appearance of better resolved ^{207}Pb-^{19}F *J*-coupling patterns.

The variable temperature spectra of α PbF_2-d is shown in Figure 6. In contrast to the spectra of α PbF_2-w, but similar to those of PbF_2-2, the spectra at room temperature and above consist of two sets of resonances: one from fluoride-ions in, or close to, the slow regime and one from ions in, or close to, the fast regime of motion. The resonance at −39.0 ppm, from ions close to the fast regime, continues to sharpen, as the temperature is raised, and increase in intensity. By 160 °C, a single resonance at −39.0 ppm is observed. The ^{207}Pb decoupled spectra at intermediate temperatures shows a gradual broadening of the F(1) and F(2) line widths due to increases in the F(1)↔F(2) exchange rates. The mobile fluoride-ions can be frozen out at lower temperatures, and at temperatures below −10 °C, only two resonances are observed at −20.5 and −57.7 ppm. More clearly resolved ^{207}Pb-^{19}F *J*-coupling patterns for the F(1) and F(2) sites are observed at lower temperatures, again confirming a decrease in fluoride-ion motion at these temperatures. Analysis of the populations and correlation times of the different regimes of motion are accomplished by line shape simulation (Table 3).

Spectra of all four α-PbF_2 samples were reproducible even after multiple variable temperature runs, indicating effects such as oxidation or changes in cation distributions did not occur to any great extent, under the conditions used to acquire the spectra.

Line Shape Simulation. To obtain more detailed information concerning the ranges of fluoride-ion correlation times present in the samples, spectral simulation was performed on

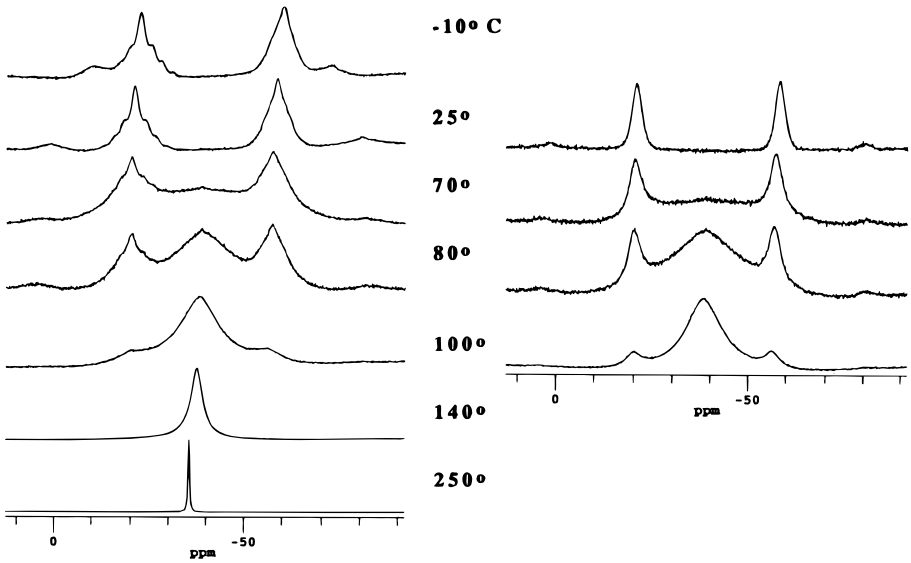

Figure 5. Variable temperature ^{19}F MAS NMR spectra of α PbF_2-w collected at −10, 25, 70, 80, 100, 140, and 250 °C at spinning speeds 20−21 kHz. ^{207}Pb decoupled ^{19}F MAS NMR spectra are shown on the right for 25, 70, 80, and 100 °C.

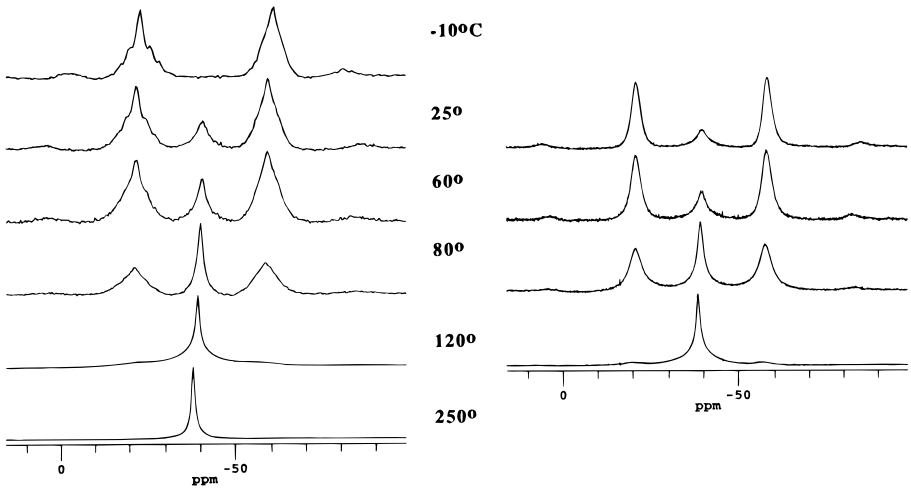

Figure 6. Variable temperature ^{19}F MAS NMR spectra of α PbF_2-d collected at −10, 25, 60, 80, 120, and 250 °C at spinning speeds 20−21 kHz. ^{207}Pb decoupled ^{19}F MAS NMR spectra are shown on the right for 25, 60, 80, and 120 °C.

the ^{207}Pb decoupled ^{19}F MAS NMR spectra. A summary of the various concentrations and correlation times for different regimes of motion obtained from representative simulations of the four samples are presented in Table 3. In cases where multiple regimes of motion were present, spectra were simulated by summing the contribution of each regime. The structural implications of these models are explored in more detail in the Discussion section.

The α-PbF_2-1 sample can be described by one set of rigid fluoride-ions at temperatures below 120 °C, with a correlation time of $\geq 4.0 \times 10^{-4}$ s. At temperatures above 120 °C, however, multiple regimes of fluoride-ion motion are required to rationalize the spectra. The low concentration of mobile fluoride-ions at 160 °C made analysis of the mobile regime difficult, and, therefore, a simple model with two narrow distributions of correlation times was used to simulate the spectrum. One set, comprising rigid fluoride-ions (F(1) and F(2)), has a correlation time of $\geq 4.0 \times 10^{-4}$ s, and the other more mobile set has a correlation time of approximately 2×10^{-5} s. At higher temperatures, the number of mobile fluoride-ions increases, and the complicated line shape can be simulated, somewhat surprisingly, with a model that contains only three correlation times. A third correlation time was required at 200 °C to account for a very small subset (0.5%) of fluoride-ions that are undergoing very fast exchange ($\tau_c = 2 \times 10^{-6}$ s), giving rise to the very small sharp peak at −39.0 ppm that is superimposed on the much broader resonance. Figure 7a,b shows the ^{207}Pb decoupled spectra of α-PbF_2-1 spectra at 200 °C and the corresponding simulation, obtained by summing the contributions from the three sets of fluoride-ions. At higher temperatures, the correlation times of the mobile fluoride-ions decrease only slightly, but the concentrations of mobile fluoride-ions increases significantly.

The variable temperature spectra of α-PbF_2-2 can be simulated with an extremely simple model, requiring only two correlation times at temperatures above 25 °C. One set of fluoride-ions (F(1) and F(2)) is rigid and has a correlation time of $\geq 5.4 \times 10^{-4}$ s (until 120 °C), i.e., the *J*-coupling is still visible, but the concentration of this set of ions drops steadily with temperature. Clearly, we are not sensitive to correlation times of greater than 5.4×10^{-4} s with this method. The second set of fluoride-ions, that gives rise to the resonance at −39.0 ppm and increases in intensity with increased temperature, can be fit well by a single Lorentzian line shape, suggesting that the mobile fluoride-ions which make up this resonance have a narrow range of correlation times. Representative simulations

Table 3. Line Shape Simulation Results[a]

sample	temp (°C)	% of total F^-	τ_c (s)
PbF_2−1	< 120	100	$\geq 4 \times 10^{-4}$
	160	87	4×10^{-4}
	160	13	2×10^{-5}
	200	74.5	3×10^{-4}
	200	25	2×10^{-5}
	200	0.5	2×10^{-6}
	250	59	3×10^{-5}
	250	40.5	1×10^{-5}
	250	0.5	2×10^{-6}
PbF_2−2	25	68	$\leq 5 \times 10^{-4}$
	25	32	$\leq 2 \times 10^{-5}$
	60	47	$\leq 5 \times 10^{-4}$
	60	53	6×10^{-6}
	100	14	$\leq 5 \times 10^{-4}$
	100	86	3×10^{-6}
PbF_2−w	25	100	3×10^{-4}
	70	45	2×10^{-4}
	70	55	3×10^{-5}
	80	30	2×10^{-4}
	80	70	2×10^{-5}
	100	14	2×10^{-4}
	100	86	2×10^{-5}
PbF_2−d	25	87	3×10^{-4}
	25	6	1×10^{-5}
	25	7	3×10^{-6}
	60	81	3×10^{-4}
	60	14	8×10^{-6}
	60	5	3×10^{-6}
	80	66	2×10^{-4}
	80	20	8×10^{-6}
	80	14	2×10^{-6}
	120	26	2×10^{-4}
	120	64	9×10^{-6}
	120	10	1×10^{-6}

[a] The percentage of fluoride-ions with corresponding correlation time are listed at various temperatures.

are shown in Table 3. Fluorine exchange rates were also calculated for the F(1) to F(2) jump process for rates close to the fast regime of motion by using eq 2.

The line shapes observed for α PbF_2-w resemble those of α PbF_2-1 except that the onset of mobility occurs at lower temperatures. Figure 8c,d shows the observed ^{207}Pb decoupled spectra and the simulated spectra of α PbF_2-w at 80 °C. The spectra were simulated by summing the contribution of two regimes of fluoride-ions with $\tau_c = 2.4 \times 10^{-5}$ and 2.0×10^{-4} s. Both regimes of fluoride-ion motion show a small gradual increase in their respective correlation times, as the temperature is increased. The fraction of the more mobile fluoride-ions increases steadily until 140 °C, when only a single Lorentzian line is observed, indicating that 100% of the fluoride-ions are now exchanging between F(1) and F(2) with a narrow range of correlation times. The difference in correlation times between the fast and slower jumping fluoride-ions in regions where both regimes are observed, is only 1 order of magnitude for α PbF_2-w and α PbF_2-1, if the very small component that contributes to 0.5% of the intensity in α PbF_2-1 is ignored. This is in contrast to α PbF_2-2 where the correlation times span 2 orders of magnitude.

The range of correlation times in α-PbF_2-d are similar to those of α-PbF_2-2; however, attempts to fit the line shapes with only two components were less successful, and a third component with an intermediate correlation time was required to improve the fit of the line shape at −39.0 ppm at temperatures between 25 and 120 °C. Figure 8d,f shows the observed and simulated spectra of α PbF_2-d at 80 °C obtained by summing the simulations obtained with three sets of correlation times: $\tau_c =$ 2.2×10^{-4}, 8×10^{-6} and 2×10^{-6} s. At temperatures above 140 °C, only a single Lorentzian line with a single correlation time was required to simulate the spectra. These simulations provide an indication of the ranges of correlation times and the percentages of fluoride-ions with motion in the different regimes. However, it is clear that a more sophisticated model that takes into account a greater range of correlation times for the mobile fluoride-ions is required to fit the α PbF_2-d spectra in particular, and the values quoted in Table 3 serve only as approximate estimates of the fraction of ions with correlation times in the different regimes of motion, at each temperature.

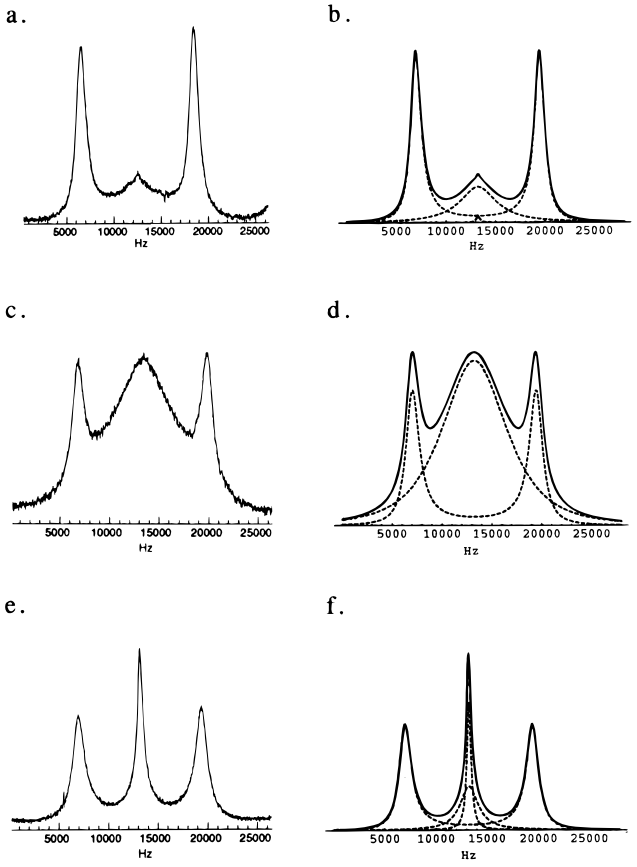

Figure 7. ^{207}Pb decoupled ^{19}F MAS NMR spectra (a, c, and e) and corresponding line shape simulations (b, d, and f). Spectra are shown for α PbF_2-1 at 200 °C (a and b), α PbF_2-w at 80 °C (c and d), and α PbF_2-d at 80 °C (e and f). Simulations were performed by summing b. three line shapes calculated with values for τ_c of 2.5×10^{-4}, 1.6×10^{-5} and 1.9×10^{-6} s, in the proportions 74.5:25:0.5, respectively, d. two line shapes with $\tau_c = 2.4 \times 10^{-5}$ s and $\tau_c = 2.0 \times 10^{-4}$ s in a ratio of 70:30, respectively, and f. three line shapes sets with correlation times $\tau_c = 2 \times 10^{-4}$, 8×10^{-6}, and 2×10^{-6} s in the proportions 66:20:14, respectively.

Two-Dimensional ^{19}F MAS Magnetization Exchange NMR. 2-D ^{19}F MAS magnetization exchange experiments were performed on α PbF_2-1 and α PbF_2-2, to probe the fluorine motion at longer time scales. Figure 8a,b shows the 2-D ^{19}F MAS magnetization exchange spectra for α PbF_2-1 and α PbF_2-2, respectively, for mixing times of 14 ms; the 1-D slices through F(1) for α PbF_2-1 and α PbF_2-2 are shown in Figure 9 (parts a and b, respectively). Cross-peaks are observed between the resonances at −20.5 and −57.7 ppm indicative of magnetization exchange between fluorine sites F(1) and F(2), but the cross-peak intensities are larger for α PbF_2-2 than for α PbF_2-1. Surprisingly, cross-peaks were not observed in α PbF_2-2 between the resonance due to the mobile fluoride-ions (−39.0 ppm) and the rigid ions (−20.5 and −57.7 ppm). Figure 10

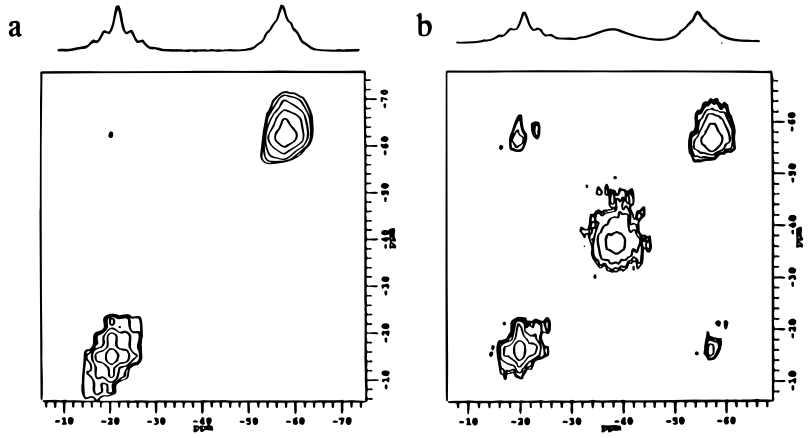

Figure 8. 2-D magnetization exchange spectra of a. α PbF_2-1 and b. α PbF_2-2 collected at spinning speeds of 20 kHz with $t_m = 14$ ms.

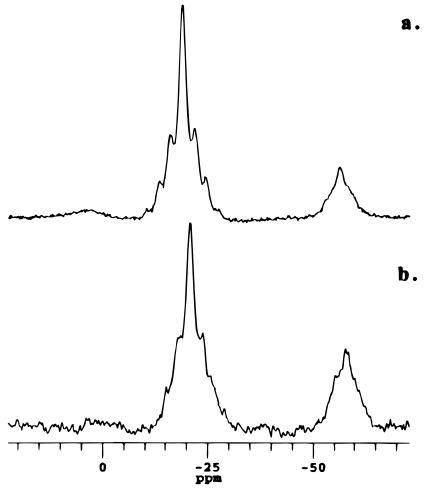

Figure 9. 1-D slices of the 2-D magnetization exchange spectra shown in Figure 8. Slices were taken parallel to ω_1 through the fluorine site F(1) for a. α PbF_2-1 and b. α PbF_2-2.

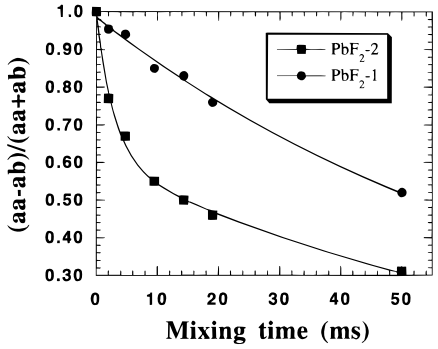

Figure 10. The plot of cross-peak intensity ratio, $(a_{AA} - a_{AB})/(a_{AA} + a_{AB})$, versus mixing time, t_m, for α PbF_2-1 and -2. Data are fit to single (PbF_2-1) and biexponential (PbF_2-2) functions (see text).

shows a plot of the cross-peak intensity as a function of the mixing time, for the two samples. The data were plotted according to eq 6. In the case of simple two-site exchange, a plot of $(a_{AA} - a_{AB})/(a_{AA} + a_{AB})$ versus mixing time, t_m, should yield an exponential curve, e^{-2ktm}, from which the exchange rate, k, can be deduced. A rapid increase in cross-peak intensity is, however, observed for α PbF_2-2 in the first 2 ms, followed by a significantly slower increase in cross-peak intensity, which cannot be fit to a single-exponential function. In contrast, the 2-D spectra of α PbF_2-1 shows a much smaller build up of cross-peak intensity as a function of mixing time, which can be fit to a single-exponential curve $y = e^{-0.0129x}$, suggesting that the magnetization exchange in α PbF_2-1 is dominated by a single rate of exchange in the range of mixing times examined. The exchange rate, k, can be deduced from the curve, giving a value of $k = 6.5$ Hz.

The exchange of magnetization between fluorine sites F(1) and F(2) may be due purely to spin diffusion (i.e., the transport of spin polarization through a network of dipolar coupled spins) or a combination of spin diffusion and fluorine chemical exchange. The plot of cross-peak intensity ratio, $(a_{AA} - a_{AB})/(a_{AA} + a_{AB})$, versus mixing time, t_m, for α PbF_2-2 can be fit quite well with the biexponential function: $y = 0.39\ e^{-0.34x} + 0.61\ e^{-0.014x}$. Thus, the magnetization exchange can be, to a first approximation, broken down into two rates of exchange: approximately 39% of the fluoride-ions undergo relatively rapid exchange (k = approximately 170 Hz) which results in the intial rapid growth in cross-peak intensity, and the remainder of the fluoride-ions undergo much slower exchange ($k = 7$ Hz). The rates of exchange for both α PbF_2-1 and α PbF_2-2 give the total rate of exchange due to either spin diffusion alone or a combination of spin diffusion and chemical exchange. Separation of the contribution from the chemical exchange and spin diffusion is extremely difficult. However, it is clear from the α PbF_2-1 data that the contribution to the total rate of magnetization exchange from spin diffusion is no more than 6.5 kHz. Thus, we can estimate a lower limit for the rate of the more mobile component observed for α PbF_2-2 of $k_{mobile} \geq 163.5$ Hz (i.e., $\tau_{mobile} \leq 6.1 \times 10^{-3}$ s). The rate of exchange of the rigid component is slightly faster for α PbF_2-2 than for α PbF_2-1, suggesting a lower limit for this exchange rate is 0.5 Hz (i.e., $\tau_{rigid} \leq 2$ s). An upper limit for the exchange rate of 7 Hz is calculated if spin diffusion is assumed to be negligible.

Discussion

Pure α PbF_2 is a moderate ionic conductor at room temperature. Studies of the bulk ionic-conductivity and the ^{19}F NMR static line widths of α PbF_2 suggest that fluoride-ion motion occurs via a vacancy diffusion mechanism.[6,17] The ^{19}F NMR spectra of α PbF_2-1, −2, -w, and -d, presented in this paper, provide a direct method of probing local mobilities and diffusion pathways of the fluoride-ions in these samples.

XPS and electron microprobe elemental analyses of α PbF_2-1 (Aldrich 99+%) showed that only lead and fluorine were present, suggesting that α PbF_2-1 is free of extrinsic dopants and, thus, is likely to contain only intrinsic defects. The ^{19}F NMR spectra show no rapid fluoride-ion exchange between or among fluorine sites at moderate temperatures (20−120 °C), which is consistent with α PbF_2's poor ionic-conductivities at

these temperatures.[6] Fluoride-ion motion was not observed until temperatures above 200 °C, where F(1)↔F(2) exchange was observed. The absence of any other resonances that can be assigned to interstitial sites is consistent with an anion-vacancy diffusion mechanism for conduction.[9] No evidence for the onset of rapid F(1)↔F(1) or F(2)↔F(2) exchange was observed prior to the onset of F(1)↔F(2) exchange: onset of motion on either the F(1) or F(2) lattice, before F(1)↔F(2) motion would first be evidenced by a narrowing of the F(1)/F(2) resonance, the removal of *J*-coupling, and at increased mobility, a reduction in spinning sidebands. It, therefore, appears that the lowest energy jump pathway in α PbF_2 occurs via F(1)↔F(2) jump processes.

The predominance of fluoride-ion diffusion via F(1)↔F(2) jump processes, rather than F(1)↔F(1) and F(2)↔F(2) jump processes, can be rationalized by considering the α PbF_2 structure. Figure 11a−c shows three orientations of the α PbF_2 local structure. Diffusion pathways can be rationalized by connecting nearest lead atoms. This results in windows through which the fluoride-ions can diffuse. The size of the windows and their proximities to the fluoride-ions will be important in controlling the activation energy and likelihood of the jump processes. Figure 11a shows the α PbF_2 structure viewed down the *y* direction. Lead and fluoride-ions are arranged in columns down the *y* axis. The lead atoms separated by 4.3 Å or less have been connected. The darkened lead−lead bonds indicate distorted square-shaped or tetragonal windows, which represent the largest lead windows in the α PbF_2 structure. All the other lead windows in the structure are smaller and triangular in shape. The arrows shown in the figure represent conduction pathways through the tetragonal windows. These different pathways are seen more clearly in Figure 11b, which shows a smaller portion of the structure, that has been rotated by approximately 90 degrees about the *z*-axis with respect to Figure 11a. There are two types of vacancies in this structure. The first, which is located on the other side of the tetragonal window from the pentacoordinate fluorine site (F2), in the F(1) columns (as viewed down the *y* direction), is also pentacoordinated. The other vacancy is tetrahedrally coordinated (cf. F(1)) and is located in the F(2) columns (Figure 11c). Examining Figure 11b more closely, the I→II and I→IV jump processes begin with a F(2) fluoride-ion first passing through the center of the tetragonal window, into the pentacoordinated vacancy site, and then through a smaller triangular window into a nearby F(1) site. The IV→V and II→III (not shown) jump processes require a jump out of the F(1) column, through a triangular shaped window into the pentacoordinated vacancy site and then through a tetragonal window to the next F(2) site. Three other possible jump processes can be discerned in Figure 11b: I→V, II→VI, and II→IV (═IV→VI). The I→V (F(2)−F(2)), II→IV, and II→VI (F(1)−F(1)) jump processes all occur by passing through two small triangular shaped windows, I→V and II→VI representing extremely long jump distances. Figure 11c depicts another view of the α PbF_2 structure, showing the F2 columns. The F(1) atoms in this figure lie above the plane of the lead triangular windows (outside the F2 column). Two other possible jump pathways (F(2)↔F(2) and F(1)↔F(2)) can be seen, which involve an initial jump into the vacant tetrahedral hole, through a triangular shaped window, followed by a second jump through another triangular window into the F(2)/F(1) site. Based only on the size of the lead windows, the F(1)↔F(2) jump processes that occur via one large tetragonal window, and through only one triangular shaped window (i.e., I→II→III, II→IV, etc.) appear to be the easiest pathway for the fluoride-ions in the close-packed structure. All these jumps occur between the F(1) and F(2) sites, which is consistent with the ^{19}F NMR spectra,

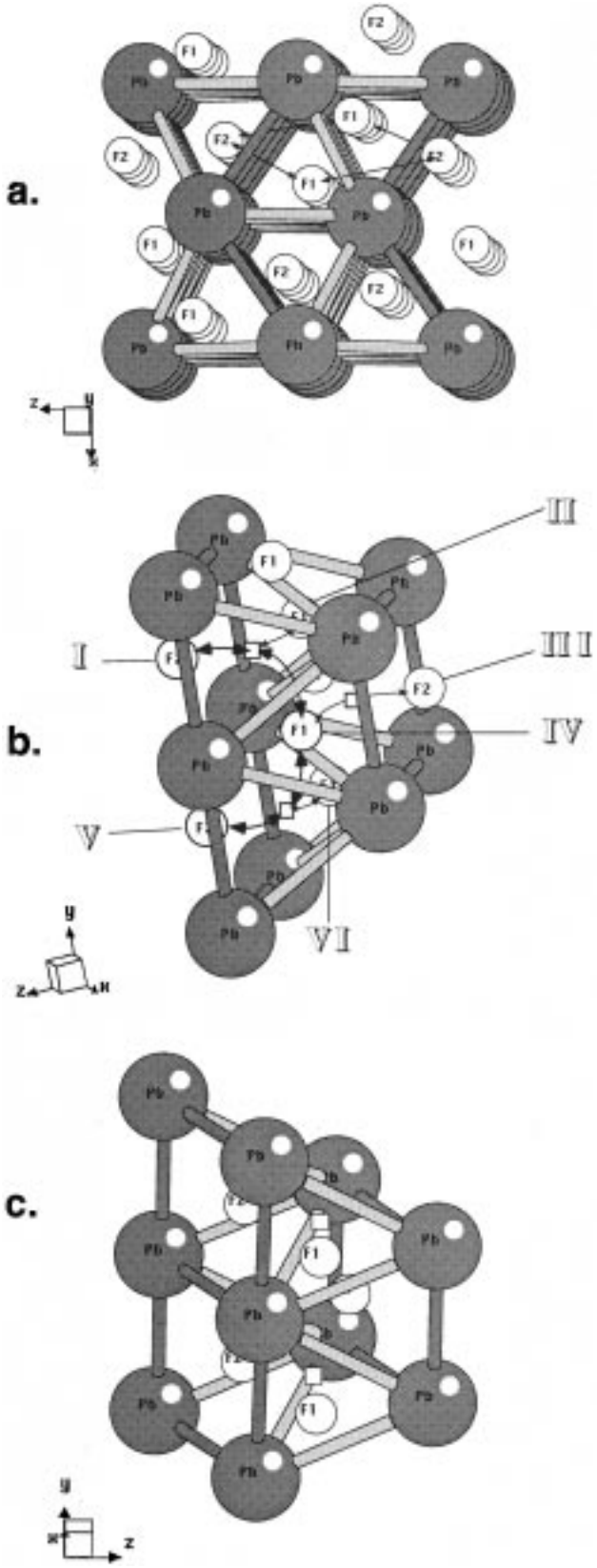

Figure 11. α PbF_2 conduction pathways, constructed by connecting lead atoms to their nearest lead neighbors: a. α PbF_2 structure viewed down *y* axis, showing low energy F(1)↔F(2) conduction pathways: shaded lead−lead connectivities indicate large tetragonal lead windows, b. expanded view of F(1) columns, and c. expanded view of F(2) columns, depicting additional jump pathways.

where no F(1)/F(1) or F(2)/F(2) motion is observed prior to the onset of F(2)/F(1) mobility. Conduction via two triangular windows, and presumably a higher energy pathway (i.e., I→V,II→VI,II→IV), is likely to be associated with longer correlation times. However, this motion is required for conduction in two and three dimensions.

A jump process in α PbF_2 depends upon the availability of an adjacent vacant site. The predominant intrinsic defect in pure α PbF_2 is likely to comprise a cation-vacancy accompanied by two anion-vacancies. Extrinsic defects, caused by, e.g., KF doping, comprise a cation defect (K^+) and an associated anion-vacancy. Intrinsic defects are likely to be spread uniformly over the solid, and, α PbF_2-1, which should predominantly contain intrinsic defects, shows a much narrower range of correlation times than α PbF_2-2, which contains extrinsic defects. As the temperature increases, the concentration of intrinsic defects increase, and the anion-vacancies diffuse more rapidly throughout the lattice, resulting in an increase in the intensity of the resonance at −39.0 ppm in the spectrum of α PbF_2-1. The small fraction of fluoride-ions in α PbF_2-1 (0.5%) seen in the spectra acquired between 200 and 250 °C, that show much shorter correlation times, may result from a small concentration of extrinsic defects.

The potassium-doped α PbF_2 samples all show increased fluoride-ion mobility in comparison to α PbF_2-1, which is consistent with an anion-vacancy conduction mechanism. The elemental analyses by electron microprobe and XPS of α PbF_2-2 show that this nominally pure material also contains significant traces of potassium. The change in concentration with sputtering time in the XPS results suggests a higher potassium concentration at the surface. This is also consistent with the reported routes used to synthesize PbF_2 commercially.[21] These all involve precipitation of PbF_2 from soluble lead and fluoride sources. Any potassium impurities in the reactants are likely to have a higher solubility than the lead reactants and products. Thus the potassium concentration is likely to be higher at the surfaces of the precipitated α PbF_2 particles.

The extrinsic doping on the surface of the α PbF_2 crystallites will lead to an increased number of vacancy defects. We propose that the large variations in correlation times in these materials are due to differences in vacancy concentrations throughout the α PbF_2 lattice. The observation of separate, narrow regimes of correlation times at intermediate temperatures, as opposed to a broad distribution of correlation times, suggests that the anion-vacancies are not uniformly spread throughout the solid but remain in close proximity to the cation-dopants (predominantly at the surface in α PbF_2-2). For example, in the spectrum of α PbF_2-2 at room temperature and above, regions containing higher concentrations of cation dopants and associated vacancies will lead to more rapidly exchanging fluoride-ions and will give rise to the resonance at −39.0 ppm. Regions with fewer or no vacant F(1) and F(2) sites will be less likely to exchange rapidly and give rise to the resonances at −20.5 and −57.7 ppm.

Vacancy/defect clustering will result from the Coulombic attractions between the oppositely charged vacancies and dopant cations. Experimental and theoretical studies on clustered defect systems such as $Ca_{1-x}Y_xF_{2-x}$ and other disordered ionic-conducting perovskite oxides have shown that clusters of defects in these systems exist and are thermodynamically stable.[1,2,22] Regions of the lattice free from extrinsic defects remain rigid at ambient temperatures. An increase in temperature, however, provides thermal energy for the vacancies to diffuse farther away from the potassium defects and creates more intrinsic defects, both of which result in a gradual increase in the intensity of the resonance at −39.0 ppm. In addition, regions of the solid containing lower concentrations of potassium dopants may start to show mobility.

Further evidence for vacancy-defect trapping or clustering comes from the room temperature 2-D magnetization exchange spectra of α PbF_2-2: cross-peaks are not observed between the resonance from the rapidly exchanging fluoride-ions and the resonances from the rigid ions, indicating a lack of chemical exchange between the two domains in the solid. The number of fluoride-ions that are initially in the mobile domain and that migrate to the rigid domain during the mixing time is negligible even after long mixing times of up to 50 ms. It is difficult to rationalize this behavior, unless the mobile region is assigned to an area in the solid with a relatively high concentration of localized defects and vacancies. The vacancies, and consequently the fluoride-ions, are mobile in an area surrounding the dopants, and the time spent by the vacancy in the dopant-free region of the solid is minimal. The 39% of the "rigid" domain of fluoride-ions that show the enhanced exchange rate, as determined from the 2-D NMR experiments of approximately 164 Hz at room temperature may be at the interfaces of the mobile and rigid regions.

The α PbF_2-d and α PbF_2-w samples also show increased fluoride-ion mobilities over that of α PbF_2-1, consistent with an increased number of vacancies produced from the extrinsic defects. Samples produced via the dry method (α PbF_2-d) are expected to contain a less even distribution of potassium throughout the α PbF_2 lattice due to some incomplete mixing. This is borne out in the ^{19}F NMR from which correlation times for fluoride-ion motion, that differ by more than 2 orders of magnitude, can be extracted. Furthermore, at intermediate temperatures, the simulations of the spectra require at least three different correlation times to achieve a reasonable fit. In contrast, the α PbF_2-w sample shows fluoride-ion mobilities characteristic of a more uniform distribution of potassium in the lattice, the difference in correlation times between the rigid and mobile fluoride-ions only spanning an order of magnitude. The room temperature ^{19}F NMR spectra of the α PbF_2-w sample does not show a resonance at −39.0 ppm, since rapid exchange at room temperature only occurs in regions of high potassium content. The distribution of the potassium is presumably such that the vacancy defects must, on average, diffuse longer distances between potassium dopants. In contrast to α PbF_2-d, the spectra can be fit with only two narrow distributions of correlation times at temperatures greater than 100 °C. The exchange rates associated with both regimes slowly increase as the temperature increases, and, at high temperature, α PbF_2-w exhibits a single resonance at −39.0 ppm that can be fit with a single Lorentzian line shape. The Lorentzian line shape signifies that all the fluoride-ions are exchanging with a very narrow distribution of correlation times, and the correlation time for the fluoride-ions at 250 °C can be calculated with eq 2 yielding a correlation time of 6.18×10^{-7} s.

The fluoride-ions associated with the regions of high mobility do not exchange rapidly with those in the rigid regions, and we propose that this is in part due to Coulombic attractions between vacancies and dopants. However, large distributions in correlation times are seen in the samples with uneven distributions of dopants, and it may be that this lack of exchange may result from variations in the concentration of potassium between the

(21) Mark, H. F.; Mcketta, J. J.; Othmer, D. F. *Encyclopedia of Chemical Technology*; Interscience Publishers: New York, 1970.

(22) Hull, S.; Wilson, C. C. *J. Solid State Chem.* **1992**, *100*, 101−114.

different crystallites, as opposed to variations in the distributions of potassium doping within the crystallites. Indeed, the behavior of α PbF_2-d, where more than one correlation time was required to model the motion of the mobile region at intermediate temperatures, indicates that this may be an important factor. However, it is difficult to rationalize the variable temperature spectra of α PbF_2-2, if this is the only cause of the lack of exchange between domains. The intensity of the resonance of the mobile fluoride-ions increases steadily with temperature, but at all temperatures the line width can be fit with a single Lorentzian, indicating a narrow range of correlation times for the mobile region. We do not see any evidence of the continuous range of correlation times that might be expected if the mobility depended on the total potassium content of the crystallite, and the variations in potassium content from crystallite to crystallite. We attempted to model the α PbF_2-2 and α PbF_2-d spectra with a Gaussian distribution of correlation times that might have been expected from this model, but we were unsuccessful in obtaining good fits to the spectra.

Conclusions

1-D ^{19}F MAS NMR, collected at spinning speeds in excess of 20 kHz, of α PbF_2 and potassium-doped α PbF_2 allows the local motion of the fluoride-ions to be probed. In all the samples examined, the spectra were consistent with lower energy conduction pathways involving F(1)↔F(2) exchange, in comparison to either F(1)↔F(1) or F(2)↔F(2) jump processes. Close examination of the α PbF_2 structure revealed a conduction pathway along the *y*-axis between F(1) and F(2) fluoride-ions involving a jump through one tetragonal and one triangular window of lead atoms, which was proposed to be the easiest conduction pathway for fluoride-ions through the solid. All other pathways involve two consecutive jumps through triangular lead windows.

The combination of one- and two-dimensional ^{19}F NMR allows a very wide range of correlation times and exchange processes to be probed with MAS methods. The spectra of α PbF_2 with a high concentration of potassium dopants at the surface or samples with uneven distributions of potassium dopants are consistent with the localization, at low temperatures, of anion vacancies around the potassium dopants; this results in fluoride-ions with two sets of correlation times for F(1)↔F(2) motion within the fluorine sublattice: one set of fluoride-ions is essentially rigid, while the second more mobile set of fluoride-ions, near the dopants, have correlation times that are approximately 2 orders of magnitude shorter. Line shape simulations allow approximate values for both the concentrations and correlation times for the mobile and rigid fluoride-ions to be extracted. 2-D magnetization exchange experiments provide further evidence for the localization of the anion vacancies at lower temperatures. The two domains of rigid and mobile fluoride ions in the surface-rich potassium-doped sample do not undergo exchange with each other, even after mixing times as long as 100 ms. The exchange rates among the rigid fluoride-ions of this sample are not, however, uniform but can be separated into two groups, with 39% of the rigid domain having an enhanced exchange rate. This enhanced exchange rate is ascribed to fluoride-ions at the interfaces between mobile and rigid regions. In the pure, or more uniformly doped samples, the vacancies are more uniformly distributed over the solid even at low temperatures, resulting in ^{19}F spectra with a smaller range of correlation times for fluoride-ion motion.

In conclusion, high speed ^{19}F MAS NMR provides a novel method for probing mechanisms for motion at the atomistic level. At the same time, the technique is also very sensitive to distributions in mobility across the whole sample. We are currently extending our 1- and 2-D ^{19}F MAS NMR studies to other fluorine ionic-conductors such as $PbSnF_4$ where diffusion rates are considerably faster and details of the conduction mechanism remain unresolved.

Acknowledgment. Support from the NSF through a grant to purchase the NMR machine (CHE-9405436) and an NYI award to C.P.G. (DMR-948017) is gratefully acknowledged.

JA972312G